Novel electrostatic MOEMS phase shifter array using CMOS-MEMS process

Jin-Chern Chiou
National Chiao Tung University
Institute of Electrical Control Engineering
Hsinchu, Taiwan 30010
and
China Medical University
School of Medicine
Taichung, Taiwan 40402

Chen-Chun Hung
Li-Jung Shieh
Zhao-Long Tsai
National Chiao Tung University
Institute of Electrical Control Engineering
Hsinchu, Taiwan 30010
E-mail: ljs.ece93g@nctu.edu.tw

Abstract. We present a 3×3 micro-optoelectromechanical systems (MOEMS) phase shifter array that achieves a $\lambda/4$ vertical displacement with peak-to-valley deformation within $\lambda/10$ (514-nm light source). The mirror reflective surface is made of an aluminum layer with a high optical reflectivity exceeding 90%. Each individual micromirror pixel is controlled and driven by comb drive actuators. The phase shifter array is fabricated using the Taiwan Semiconductor Manufacturing Company 0.35-μm 2P4M complementary metal-oxide semiconductor process. In-house post-processing is utilized to reserve a 40-μm-thick bulk-silicon under the 200 μm$\times$200 μm mirror. This eliminates mirror deformation from residual stress after the device is released. The micromirror demonstrates a vertical displacement of $\lambda/4$ at 38 V. The device resonant frequency is 3.71 kHz, and the fill factor is 0.65. This MOEMS phase shifter array can be used as a spatial light modulator in holographic data storage systems. © *2010 Society of Photo-Optical Instrumentation Engineers.* [DOI: 10.1117/1.3280264]

Subject terms: complementary metal-oxide semiconductor–microelectromechanical systems; phase shifter; micro-optoelectromechanical systems; comb drive actuator; micromirror.

Paper 09127R received Aug. 3, 2009; revised manuscript received Nov. 5, 2009; accepted for publication Nov. 9, 2009; published online Jan. 19, 2010.

1 Introduction

Micro-optoelectromechanical systems (MOEMS) have flourished over the last decade by leveraging IC microfabrication technology.[1] Their applications included projection displays,[2] optical scanners,[3] and imaging systems.[4] Among these devices, the MOEMS phase shifter plays an important role in the light-diffraction interference. If a phase shifter can be operated in in-phase mode (0-deg phase difference) and out-of-phase mode (180-deg phase difference), respectively, the capacity of a holographic data storage system can be increased by double. Furthermore, this capacity can be increased by 2^N times when N phase shifters are in the system.[5,6]

Among the existing actuation methods for MOEMS mirrors that were previously proposed are thermal, piezoelectric, and electrostatic principles. Thermal actuation is based on the difference between the thermal expansions of different materials in a bimorphic actuation structure. Although this excitation principle is easily implemented, it requires high power consumption.[7] Note that a typical thermal actuator can be used for applications that require large displacement.[3] Piezoelectric actuation is frequently used to drive micromirrors that need precision. However, piezoelectric materials may cause hysteresis and are incompatible with the complementary metal-oxide semiconductor (CMOS) process.[8–10] Electrostatic actuation is the most widely used method in fabricating micromachined mirrors.[11–14] The main benefit of electrostatic actuation is due to its low power consumption and submicrometer displacement in optical devices. Interferometry using an electrostatic-driven microactuator can precisely control displacements in the nanometer range, and the required actuation force is usually low.[15] Recently, many electrostatic actuation methods have been developed, such as the parallel plate, lateral comb drive, and vertical comb drive structures. Vertical out-of-plane motion micromirrors with a parallel plate electrostatic actuator have a nonlinear pull-in phenomenon, which severely constrains the stable region at one-third the length of the gap.[16,17] Electrostatic comb drive actuators were developed to avoid pull-in. Numbers of optical applications using electrostatic comb drive micromirror have been demonstrated, such as optical scanners,[18,19] phase-shifting interferometers,[20] and laser displays.[21]

In addition to the previously mentioned actuation methods, micromirror flatness is also an important issue when designing MOEMS mirrors. Micromirrors made of thin film materials usually have a curved surface due to residual stress once the structure is released.[22,23] Stress-induced out-of-plane deformation must be small compared to the optical wavelength to avoid adversely affecting device performance. Thus, a number of methods have been proposed to eliminate curvature or reduce residual stress of the micromirrors. For example, a thick bulk-silicon micromirror fabricated via the deep reactive-ion etching (DRIE) process can overcome the nonplanarity of CMOS thin film microstructures.[24] Moreover, bombarding the microstructure surface with ions provides another method to modify the residual stress gradient.[25,26]

In order to effectively overcome the previously mentioned drawbacks in fabricating micromirrors, this work develops a MOEMS phase-shifting micromirror array that can achieve a $\lambda/4$ vertical displacement and a mirror peak-to-

1932-5150/2010/$25.00 © 2010 SPIE

Downloaded From: http://nanolithography.spiedigitallibrary.org/ on 04/25/2014 Terms of Use: http://spiedl.org/terms

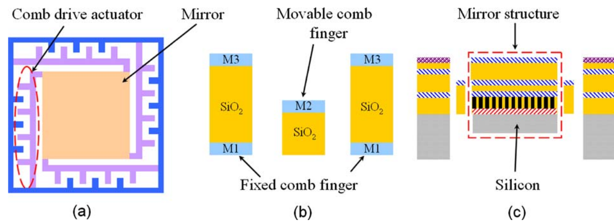

Fig. 1 Schematic of the individual mirror pixel: (a) top view, (b) cross section of the comb fingers, and (c) cross section.

valley deformation within λ/10. Electrostatic comb actuators are employed to drive each individual mirror pixel. The standard CMOS process and in-house post-CMOS process are utilized to fabricate the device. The following sections described the device design, theoretical analysis, simulation results, and fabrication processes. Experimental results have shown that the micromirror had a vertical displacement of λ/4 at 38 V with resonant frequency at 3.71 kHz.

2 Design of the MOEMS Phase Shifter

The MOEMS phase-shifting micromirror array is fabricated by the Taiwan Semiconductor Manufacturing Company (TSMC) standard 0.35-μm double polysilicon quadruple metal (2P4M) CMOS process.[27] The micromirror is designed to achieve a λ/4 vertical displacement for a 514-nm wavelength light source. Figure 1(a) shows a schematic drawing of an individual mirror pixel. It consists of a 200 μm × 200 μm micromirror structure and four sets of comb fingers. The micromirror is supported by four suspension beams. The comb fingers are designed along the suspension beams, acting as movable and fixed comb fingers. One end of the beams is fixed to an anchor, and the other end is attached to the micromirror. The mirror reflective surface is an aluminum metal layer with a high optical reflectivity exceeding 90%. Figure 1(b) shows a cross-sectional view of the vertical comb drive actuator. The fixed comb fingers comprise M1, M3, and silicon dioxide, and the movable comb fingers are made of M2 and silicon dioxide. When a voltage is applied between the movable comb (M2) and fixed comb (M3), the micromirror can be pulled upward by the electrostatic force induced by the fringe effect. Conversely, the micromirror can be pulled downward when driving voltage applied to the fixed comb is changed from M3 to M1. Thus, the multilayer structure provides vertical motion capability.

A bulk-silicon under the micromirror is reserved for reducing mirror deformation due to residual stress after the structure is released, as illustrated in Fig. 1(c). The thickness of bulk-silicon is estimated according to the design specification that mirror peak-to-valley deformation is within λ/10 (51 nm). In order to design the thickness of bulk-silicon, the curvature model is used for estimation purpose. The curvature of a micromirror is defined as:[28]

$$\rho = \frac{\ell^2}{2d}, \tag{1}$$

where ρ is the radius of curvature, ℓ is the half length of micromirror, and d is the mirror peak-to-valley deformation. Thus, ρ must be larger than 100 mm to satisfy d within λ/10. Note that the beam curvature model can also be used to estimate the thickness of bulk-silicon. Since a bowl-shape micromirror is created upon completing the release process, the free center point can be regarded as an anchor with four fixed ends that are connected to the suspension beams treated as free ends. This is similar to the case where the composite beam is bent by residual stress.

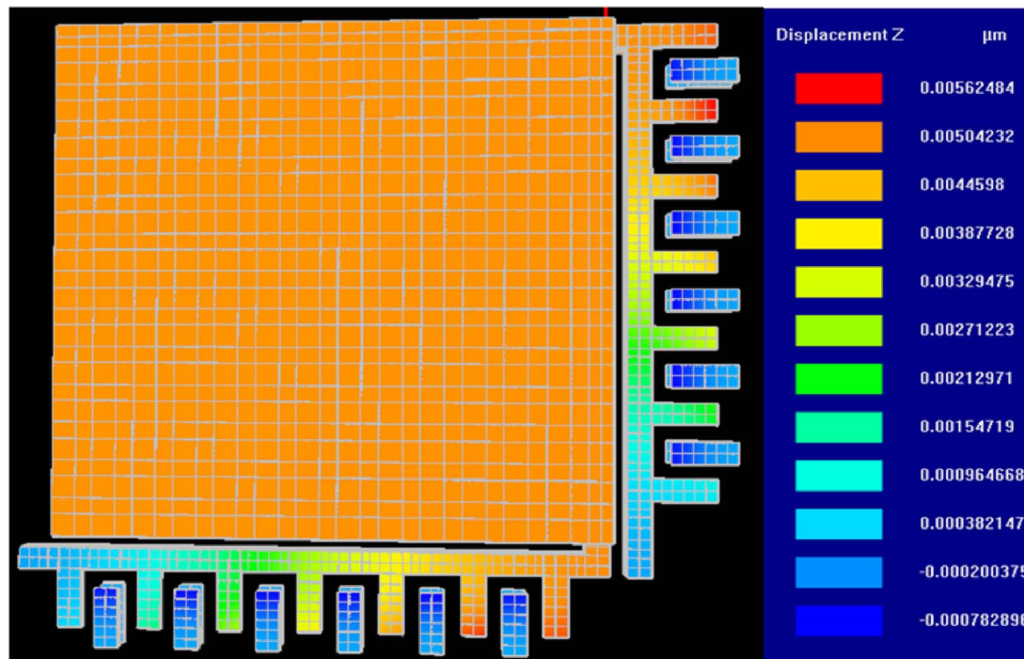

Fig. 2 Deformation of the simplified micromirror model with 70-V dc bias voltage.

Downloaded From: http://nanolithography.spiedigitallibrary.org/ on 04/25/2014 Terms of Use: http://spiedl.org/terms

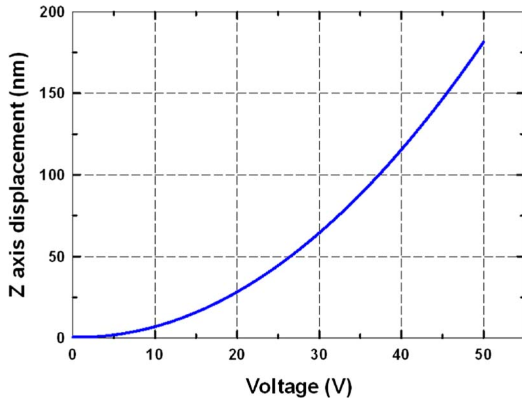

Fig. 3 Simulation result of z-axis displacement versus driving voltage.

Therefore, the curvature of the micromirror also can be expressed as:[29]

$$\frac{1}{\rho} = \frac{6(m \cdot \sigma_B - \sigma_A)}{h \cdot E_B \cdot [3 \cdot m + K/q \cdot (1+q)^2]}, \tag{2}$$

where σ_A and σ_B are the residual stresses of materials A and B. E_A and E_B are the Young's modulus of materials A and B. Symbols $m=(E_A/E_B)$, $q=(t_A/t_B)$, $h=t_A+t_B$, and K is denoted as:

$$K = 1 + 4 \cdot m \cdot q + 6 \cdot m \cdot q^2 + 4 \cdot m \cdot q^3 + m^2 \cdot q^2, \tag{3}$$

where t_A and t_B are the thicknesses of materials A and B. K is a material coefficient of materials A and B. The material A in the micromirror structure denotes silicon substrate, and material B all used layers in CMOS process besides silicon. The material properties are taken from the National Chip Implementation Center (CIC).[30] Notably, silicon residual stress (σ_A) is neglected due to the bulk-silicon, which is reserved for reducing mirror deformation treated as rigid body. Therefore, using Eqs (1) and (2), the thickness of bulk-silicon (t_A) can be calculated. The calculation result indicates that t_A have to be larger than 35-μm for satisfying the mirror peak-to-valley deformation within $\lambda/10$. To consider post-CMOS process variations, a 40-μm-thick bulk-silicon is reserved in the design.

3 Theoretical Analysis and Field Emission Microscopy (FEM) Simulation

3.1 *Static Behavior*

Vertical motion of an electrostatic comb drive actuator occurs when a driving voltage is applied between the fixed and movable comb fingers. The electrostatic force is given by

$$F = \frac{1}{2} N \frac{\mathrm{d}C}{\mathrm{d}z} V^2, \tag{4}$$

where N is the number of comb fingers, C is the capacitance of comb fingers, z is the displacement of movable fingers, and V is the applied dc bias voltage. For a comb finger pair, $\mathrm{d}C/\mathrm{d}z$ can be expressed as

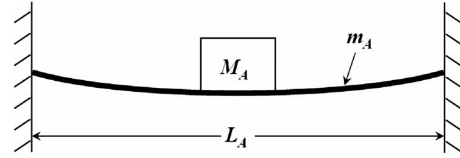

Fig. 4 Diagram of clamped-clamped beam with a center mass.

$$\frac{\mathrm{d}C}{\mathrm{d}z} = \frac{\varepsilon L}{g}, \tag{5}$$

where ε is the dielectric constant in air, L is the finger length, and g is the gap between fingers. By using Eq. (5) in Eq. (4), electrostatic force can be rewritten as a function of applied voltage.

To understand the static behaviors of the device, an FEM simulator, IntelliSuite, is utilized to simulate micromirror deformation and displacement. Figure 2 shows the simulation result of a simplified model for a quarter micromirror with a driving voltage of 70 V. Micromirror displacement is clearly the same with the free end of the suspension beams. That is, deformation of the suspension beams induced by the electrostatic force can fully pass to the micromirror and lead to a vertical levitation of the micromirror. Figure 3 plots micromirror displacement versus driving voltage. The simulation result demonstrates that the micromirror can achieve a 128-nm $(\lambda/4)$ vertical displacement when applied voltage is about 42 V.

3.2 *Resonant Frequency*

A simplified theoretical model is employed to calculate the resonant frequency of the proposed micromirror device. Deformation of the suspension beams induced by an electrostatic force leads to a vertical levitation of the micromirror. Thus, the device model is similar to that of a clamped-clamped beam with a center mass, as illustrated in Fig. 4. Four suspension beams can be regarded as two sets of equivalent beams acting as a clamped-clamped beam. The fundamental resonant frequency of the equivalent model is expressed as:[31]

$$f = \frac{4}{\pi} \left[\frac{3 \times \Sigma_{i=1}^{N} E_i I_i}{L_A^3 (M_A + 0.37 m_A)} \right]^{1/2}, \tag{6}$$

where N is the number of layers in the suspension beam; E_i and I_i are the Young's modulus and the moment of inertia of each layer, respectively; L_A and m_A are the length and the mass of the equivalent clamped-clamped beam, respectively; and M_A is micromirror mass. The theoretical resonant frequency derived by Eq. (6) is 3.98 kHz. On the other hand, resonant frequency is also simulated using IntelliSuite. Notably, the FEM simulations require only a movable comb, suspension beams, and a micromirror to calculate the resonant frequency. The simulation result indicates that the fundamental resonant frequency is about 4.15 kHz and the mode shape is vertical motion. These results can be used as the reference data in actual experimental measurements.

Downloaded From: http://nanolithography.spiedigitallibrary.org/ on 04/25/2014 Terms of Use: http://spiedl.org/terms

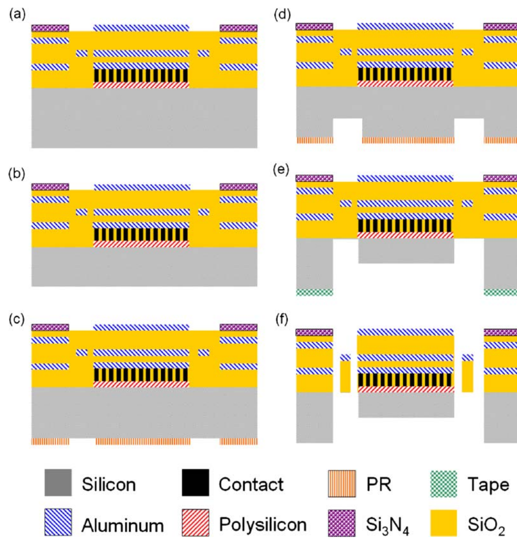

Fig. 5 Post-CMOS fabrication process flow: (a) completion of CMOS process, (b) reserving only 100 μm of silicon by grinding process, (c) defining proof mass area by backside lithography process, (d) first backside ICP etching step, (e) second backside ICP etching step, and (f) frontside anisotropic RIE etching process to release suspended microstructures.

4 Fabrication

The proposed MOEMS phase shifter was fabricated by the TSMC 0.35-μm 2P4M CMOS process, which was provided by the National Chip Implementation Center (CIC)[27] and a self-designed post-CMOS process. The CMOS process consists of two polysilicon layers, four metal layers, three via layers, and several dielectric layers. All metal layers are made of aluminum, and the contact/via holes are filled with tungsten plugs. The dielectric layers are silicon dioxide, and the passivation layer includes silicon dioxide and silicon nitride. The etched holes are filled with silicon dioxide. In order to fabricate a flat plane surface, chemical mechanical polishing (CMP) is employed after each deposition layer was completed.

After the CMOS foundry process, all MEMS structures are still connected with the silicon substrate. Notably for the device releasing issue, the passivation window of the MEMS structure must be opened in advance of post-processinng. The self-designed post-CMOS process is applied to reserve a bulk-silicon mass for reducing micromirror deformation and release the suspended structures. The post-process includes one grinding process, one backside alignment photography, a two-step backside inductively coupled plasma (ICP) etching process, and a frontside reactive ion etch (RIE) step. Figure 5 illustrates the post-process flow. Figure 5(a) shows the device fabricated after the CMOS foundry process with the passivation window already open. A backside grinding process is then utilized to grind down the silicon substrate thickness, reversing only 100 μm for economic considerations, as shown in Fig. 5(b). After that, a backside lithography process is applied to define the proof mass area, and then the first anisotropic ICP etching step is utilized to etch the silicon substrate for proof mass reservation, in which photo-resister (PR) is used as the hard mask, as illustrated in Fig. 5(c) and 5(d). Figure 5(e) displays the second step in the ICP etching process. The polyimide tape (PI tape) is applied as the mask instead of PR. Although the ICP process will etch the PI tape, it will extend the etching time to form the proof mass. In this etching step, silicon dioxide is utilized as the etching stop layer because the etching selectivity of silicon dioxide is significantly higher than that of PI tape. Last, a frontside anisotropic RIE etching process is used to release the micromirror device, as shown in Fig. 5(f). Figure 6 displays scanning electron microscope (SEM) images of the device fabricated using the CMOS process and post-CMOS processes.

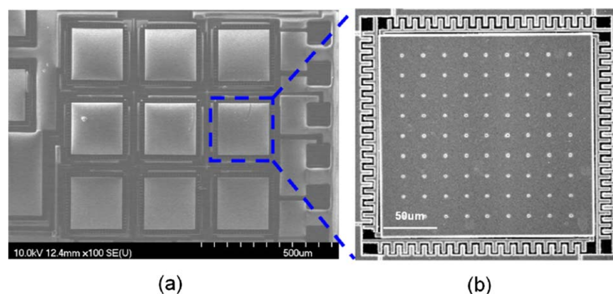

Fig. 6 SEM pictures of MOEMS phase shifter: (a) 3×3 array, and (b) an individual mirror pixel.

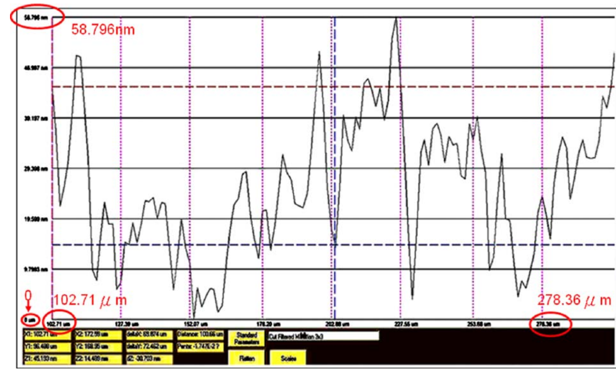

Fig. 7 Surface flatness of the micromirror device.

5 Experimental Results

5.1 *Flatness of the Micromirror*

In order to examine micromirror flatness, a white light interferometer (WYKO NT1100 system) is used for the preliminary measurement. Micromirror flatness is an important issue in phase shifter applications. The x and y directions of the micromirror surface are scanned. Figure 7 shows the x direction roughness scanned at 200-μm distance from one side, passing through the mirror center to the other side. The measurement result demonstrates that roughness only about 60 nm and no mirror deformation occurred in this device. Deformation induced by residual stress from the CMOS process is totally eliminated because the curve is distributed uniformly and does not gather on any side of the mirror. A similar scanning result is obtained for the y direction. Thus, mirror peak-to-valley deformation conforms to the optical specification.

Downloaded From: http://nanolithography.spiedigitallibrary.org/ on 04/25/2014 Terms of Use: http://spiedl.org/terms

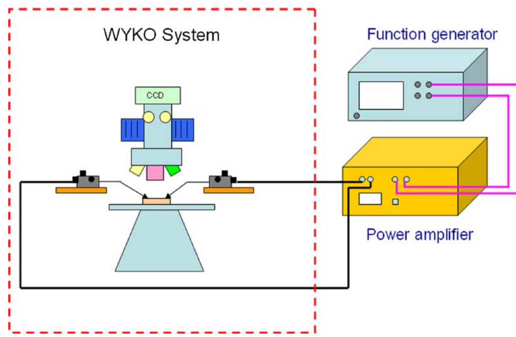

Fig. 8 Experimental diagram of the static characteristic measurement.

5.2 *Static Characteristic Measurement*

The WYKO interferometer is also used for static characteristic measurement. Figure 8 shows the experimental setup. A dc bias voltage provided by the power amplifier is utilized to actuate the MOEMS phase shifter. Figure 9 compares simulation and measurement results for vertical displacement versus driving voltage. The experimental result demonstrates that vertical motion of the micromirror can achieve a 128-nm displacement ($\lambda/4$ of the 514-nm light source) when 38 V is applied to the comb actuator. The vertical displacement of the micromirror of 0 to 128 μm is obtained by increasing the driving voltage from 0 to 38 V; thus, the requirement of $\lambda/4$ displacement can easily be reached less than 40 V. Figure 10 displays the WYKO interferometer image of a mirror pixel before [Fig. 10(a)] and after [Fig. 10(b)] actuation with 38 V. It is clear that a 180 deg phase difference is observed. This result shows that the micromirror achieves a $\lambda/4$ vertical displacement precisely.

5.3 *Frequency Response Measurement*

Figure 11 shows the frequency response of the micromirror device measured by using an MEMS motion analyzer (MMA). The micromirror is biased by a sinusoidal wave with voltages offset of 30 V and amplitude of 5 V, and the frequency ranges between 2 and 5 kHz. The first resonant frequency mode is measured at 3.71 kHz, and it closely matches the calculation (3.98 kHz) and simulation result (4.15 kHz). The error is due to variations of the CMOS fabrication process and post-process. The quality factor of the mirrors is 41.

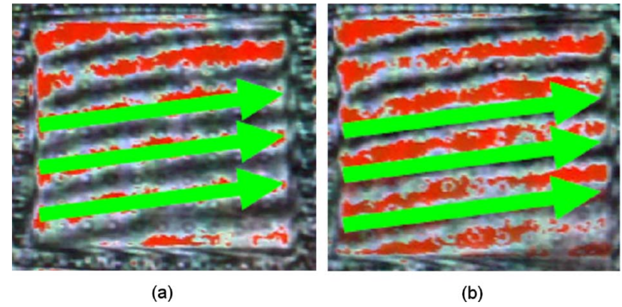

Fig. 10 WYKO interferometer images of a mirror pixel: (a) before actuation, and (b) after actuation with 38 V.

6 Conclusions

This work presents a 3×3 electrostatic MOEMS phase shifter array fabricated by TSMC 0.35-μm 2P4M CMOS process and the self-designed post-CMOS process. The individual mirror pixel is 200 μm$\times$200 μm. Mirror deformation resulting from residual stress of the CMOS process is eliminated via proof mass reservation design. The design, modeling, simulation, and measurement are presented. Preliminary measurement results demonstrate that the micromirror can achieve a 128-nm ($\lambda/4$) vertical displacement with a driving voltage of 38 V and that the resonant frequency is 3.71 kHz. This MOEMS phase shifter array has potential as a spatial light modulator (SLM) in holographic data storage systems in the future.

Acknowledgments

This work was supported in part by the Ministry of Economic Affairs, Taiwan, under Contract No. 96-EC-17-A-07-S1-011, and the National Science Council, Taiwan, under Contract No. NSC-96–2218-E-009–001 and NSC-98–2218–E-039–001. It was also supported in part by Department of Health, Taiwan, Clinical Trial and Research Center of Excellence and Raydium Semiconductor Corporation under Contract No. 098426N3. The authors also would like to thank the National Chip Implementation Center (CIC) for technical support.

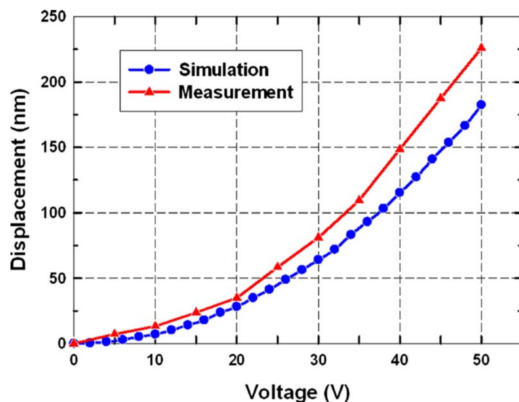

Fig. 9 Static characteristic of the micromirror.

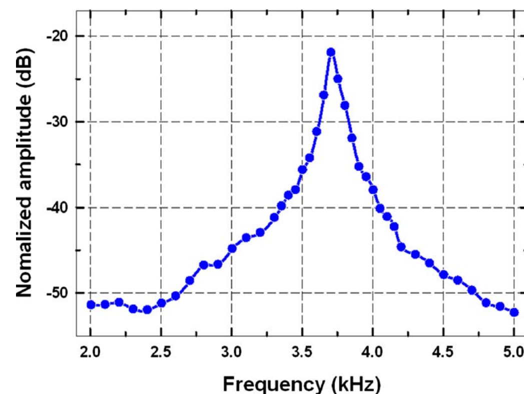

Fig. 11 Frequency response of the micromirror.

Downloaded From: http://nanolithography.spiedigitallibrary.org/ on 04/25/2014 Terms of Use: http://spiedl.org/terms

References

1. S. Kim, G. Barbastathis, and H. L. Tuller, "MEMS for optical functionality," *J. Electroceram.* **12**(1), 133–144 (2004).
2. P. F. Van Kessel, L. J. Hornbeck, R. E. Meier, and M. R. Douglass, "A MEMS-based projection display," *Proc. IEEE* **86**(8), 1687–1704 (1998).
3. A. Jain, H. Qu, S. Todd, and H. Xie, "A thermal bimorph micromirror with large bidirectional and vertical actuation," *Sens. Actuators, A* **122**(1), 9–15 (2005).
4. H. Xie, Y. Pan, and G. K. Fedder, "Endoscopic optical coherence tomographic imaging with a CMOS-MEMS micromirror," *Sens. Actuators, A* **103**(1–2), 237–241 (2003).
5. K. Anderson and K. Curtis, "Polytopic multiplexing," *Opt. Lett.* **29**(12), 1402–1404 (2004).
6. H. Horimai and X. Tan, "Advanced collinear holography," *Opt. Rev.* **12**(2), 90–92 (2005).
7. A. Tuantranont, L. A. Liew, V. M. Bright, W. Zhang, and Y. C. Lee, "Phase-only micromirror array fabricated by standard CMOS process," *Sens. Actuators, A* **89**(1–2), 124–134 (2001).
8. F. Filhol, E. Defay, C. Divoux, C. Zinck, and M. T. Delaye, "Resonant micro-mirror excited by a thin-film piezoelectric actuator for fast optical beam scanning," *Sens. Actuators, A* **123–124**, 483–489 (2005).
9. I. Kanno, T. Kunisawa, T. Suzuki, and H. Kotera, "Development of deformable mirror composed of piezoelectric thin films for adaptive optics," *IEEE J. Sel. Top. Quantum Electron.* **13**(2), 155–161 (2007).
10. X. H. Xu, Y. Feng, B. Q. Li, and B. R. Chu, "Integration of displacement sensor into bulk PZT thick film actuator for MEMS deformable mirror," *Sens. Actuators, A* **147**, 242–247 (2008).
11. W. G. Wu, Q. H. Chen, G. Z. Yan, D. Q. Yin, Z. Y. Chen, Y. L. Hao, A. S. Xu, and Y. Y. Wang, "Micro torsion mirror actuated by compound electrostatic driving structure," *Sens. Actuators, A* **135**(2), 758–764 (2007).
12. T. Fleischmann, K. Kubota, P. O. Vaccaro, T. S. Wang, S. Saravanan, and N. Saito, "Self-assembling GaAs mirror with electrostatic actuation using micro-origami," *Physica E (Amsterdam)* **24**(1–2), 78–81 (2004).
13. C. H. Ji, M. Choi, S. C. Kim, S. H. Lee, S. H. Kim, Y. Yee, and J. U. Bu, "An electrostatic scanning micromirror with diaphragm mirror plate and diamond-shaped reinforcement frame," *J. Micromech. Microeng.* **16**(5), 1033–1039 (2006).
14. F. R. Hu, J. Yao, C. K. Qiu, and D. J. Wang, "A new design of large stroke micro-deformable mirror actuated by electrostatic repulsive force," in *Proc. 2nd Int. Conf. Integration and Commercialization of Micro and Nanosystems (MicroNano08)*, pp. 117–120 (2008).
15. A. P. Lee, C. F. McConaghy, G. Sommargren, P. Krulevitch, and E. W. Campbell, "Vertical-actuated electrostatic comb drive with *in situ* capacitive position correction for application in phase shifting diffraction interferometry," *J. Microelectromech. Syst.* **12**(6), 960–971 (2003).
16. J. Pons-Nin, A. Rodriguez, and L. M. Castaner, "Voltage and pull-in time in current drive of electrostatic actuators," *J. Microelectromech. Syst.* **11**(3), 196–205 (2002).
17. N. Sabate, R. Rubio, C. Calaza, J. Santander, L. Fonseca, I. Gracia, C. Cane, M. Moreno, and S. Marco, "Mirror electrostatic actuation of a medium-infrared tunable Fabry-Perot interferometer based on a surface micromachining process," *Sens. Actuators, A* **123–124**, 584–589 (2005).
18. D. Hah, C. A. Choi, C. K. Kim, and C. H. Jun, "A self-aligned vertical comb-drive actuator on an SOI wafer for a 2D scanning micromirror," *J. Micromech. Microeng.* **14**(8), 1148–1156 (2004).
19. M. H. Kiang, O. Solgaard, R. S. Muller, and K. Y. Lau, "Surface-micromachined electrostatic-comb driven scanning micromirrors for barcode scanners," in *Proc. IEEE MEMS '96*, pp. 192–197 (1996).
20. H. Choo, R. Kant, D. Garmire, J. Demmel, and R. S. Muller, "Fast, MEMS-based, phase-shifting interferometer," in *Proc. Solid-State Sensor and Actuator Workshop*, pp. 94–95 (2006).
21. Y. C. Ko, J. W. Cho, Y. K. Mun, H. G. Jeong, W. K. Choi, J. W. Kim, Y. H. Park, J. B. Yoo, and J. H. Lee, "Eye-type scanning mirror with dual vertical combs for laser display," *Sens. Actuators, A* **126**(1), 218–226 (2006).
22. J. L. A. Yeh, H. Jiang, and N. C. Tien, "Integrated polysilicon and DRIE bulk silicon micromachining for an electrostatic torsional actuator," *J. Microelectromech. Syst.* **8**(4), 456–465 (1999).
23. R. R. A. Syms, "Surface tension powered self-assembly of 3-D micro-optomechanical structures," *J. Microelectromech. Syst.* **8**(4), 448–455 (1999).
24. H. Xie, Y. Pan, and G. K. Fedder, "A CMOS-MEMS mirror with curled-hinge comb drives," *J. Microelectromech. Syst.* **12**(4), 450–457 (2003).
25. R. Nowak, Y. Miyagawa, C. L. Li, S. Nakao, S. Maruno, and S. Miyagawa, "Post-deposition reduction of internal stress in thin films: the case of HfN coatings bombarded with Au ions," *Mater. Lett.* **33**(1–2), 31–36 (1997).
26. T. G. Bifano, H. T. Johnson, P. Bierden, and R. K. Mali, "Elimination of stress-induced curvature in thin-film structures," *J. Microelectromech. Syst.* **11**(5), 592–597 (2002).
27. "CIC CMOS MEMS Design Platform for Heterogeneous Integration," Document No. CIC-CID-RD-08-01 Chip Implementation Center, CIC, Taiwan (2008).
28. B. Mi, D. A. Smith, H. Kahn, F. L. Merat, A. Heuer, and S. M. Phillips, "Static and electrically actuated shaped MEMS mirrors," *J. Microelectromech. Syst.* **14**(1), 29–36 (2005).
29. R. T. Chen, H. Nguyen, and M. C. Wu, "A low voltage micromachined optical switch by stress-induced bending," in *Proc. IEEE MEMS '99*, pp. 424–428 (1999).
30. National Applied Research Laboratories, National Chip Implementation Center, Hsinchu Science Park, Taiwan, http://www.cic.org.tw.
31. R. D. Blevins, *Formulas for Natural Frequency and Mode Shape*, Krieger, Malabar, pp. 156–160 (1984).

Jin-Chern Chiou received MS and PhD degrees in aerospace engineering science from the University of Colorado at Boulder in 1986 and 1990, respectively. Before joining the Department of Electrical and Control Engineering, National Chiao Tung University, Taiwan, in 1992, he worked at the Center for Space Structure and Control, University of Colorado, Boulder, as a research associate. His research interests include microelectromechanical systems (MEMS), biosensors, servo control, and modeling and control of multibody dynamic systems (MBDs). Currently, Dr. Chiou is a professor in the Department of Electrical Engineering, National Chiao Tung University, director of the Biomedical Engineering Research and Development Center of China Medical University, and task force leader of the National Science and Technology Program for SOC.

Chen-Chun Hung received his BS in automatic control engineering from Feng Chia University, Taichung, Taiwan, in 1998 and an MS from the Department of Engineering and System Science at National Tsing Hua University, Hsinchu, Taiwan, in 2003. He is currently working toward a PhD, and his research interests are in the area of SOG processes, MEMS decoupling actuators, and micro hot-embossing biomedical sensors.

Li-Jung Shieh received his BS in automatic control engineering from Feng Chia University, Taichung, Taiwan, in 1997 and an MS from the Department of Engineering and System Science at National Tsing Hua University, Hsinchu, Taiwan, in 2004. He is currently working toward a PhD, and his research interests are in the area of CMOS-MEMS sensors and actuators.

Zhao-Long Tsai received his BS in power mechanical engineering from National Tsing Hua University, Hsinchu, Taiwan, in 2006 and an MS in electrical and control engineering from National Chiao Tung University, Hsinchu, Taiwan, in 2008. He is currently serving in the Taiwan Marine Corps. His research interests include microelectromechanical systems (MEMS) design and applications.

Downloaded From: http://nanolithography.spiedigitallibrary.org/ on 04/25/2014 Terms of Use: http://spiedl.org/terms